

UNIVERSIDADE ESTADUAL DE CAMPINAS  
SISTEMA DE BIBLIOTECAS DA UNICAMP  
REPOSITÓRIO DA PRODUÇÃO CIENTÍFICA E INTELLECTUAL DA UNICAMP

**Versão do arquivo anexado / Version of attached file:**

Versão do Editor / Published Version

**Mais informações no site da editora / Further information on publisher's website:**

<https://www.sciencedirect.com/science/article/pii/S0963996919302297>

**DOI: 10.1016/j.foodres.2019.04.006**

**Direitos autorais / Publisher's copyright statement:**

©2019 by Pergamon Press. All rights reserved.

DIRETORIA DE TRATAMENTO DA INFORMAÇÃO

Cidade Universitária Zeferino Vaz Barão Geraldo

CEP 13083-970 – Campinas SP

Fone: (19) 3521-6493

<http://www.repositorio.unicamp.br>



## Physical approach for a quantitative analysis of the phytosterols in free phytosterol-oil blends by X-ray Rietveld method

Gomes Silva M.<sup>a,\*</sup>, Santos V.S.<sup>b</sup>, Fernandes G.D.<sup>a</sup>, Calligaris G.A.<sup>c</sup>, Santana M.H.A.<sup>b</sup>, Cardoso L.P.<sup>c</sup>, Ribeiro A.P.B.<sup>a</sup>

<sup>a</sup> Department of Food Technology, School of Food Engineering, University of Campinas, 80 Monteiro Lobato St., Campinas, SP 13083-970, Brazil

<sup>b</sup> Department of Biotechnological Processes, School of Chemical Engineering, University of Campinas, 500 Albert Einstein Ave., Campinas, SP 13083-970, Brazil

<sup>c</sup> Department of Applied Physics, Institute of Physics Gleb Wataghin, University of Campinas, 777 Sérgio Buarque de Holanda St., Campinas, SP 13083-859, Brazil



### ARTICLE INFO

#### Keywords:

Lipids  
Free Phytosterols  
Rietveld method  
Polymorphism  
Crystallization  
Thermal properties

### ABSTRACT

This study investigates and compares the thermal phase transition and crystallization characteristics of a commercial food grade free phytosterol blend (FP) with a stigmasterol analytical standard (SS), the FP behavior in a food model system after its addition to high oleic sunflower oil (HOSO). The properties of the FP:HOSO blends were studied by differential scanning calorimetry, solid content, crystal morphology, and X-ray diffraction (XRD) measurements. The Rietveld method (RM) was applied associated with the XRD measurements to support phase analysis and the study of crystallinity degree. The materials were also characterized by means of chemical composition, such as fatty acids and triacylglycerol profiles, for HOSO, and phytosterol profile, for FP. Regarding phase behavior and crystallinity properties, FP has very similar characteristics to SS. The thermal behavior of FP:HOSO blends has two characteristic peaks, one from FP and the other from HOSO. The similarity reported in the literature between the diffraction pattern of FP and pure phytosterols is a positive characteristic for FP. A high FP concentration resulted in high supersaturation and thus the formation of small crystals. The incorporation of HOSO reduced of the large agglomeration of FP crystals and the dispersion crystalline aggregates (spherulites) of FP crystals. The application of RM in FP:HOSO blends to quantify the crystalline and amorphous phases was successfully used. The application has provided the expected value for these phases, according to the same experimental mass ratio of the blends, thereby validating the applicability of this approach in this type of material.

### 1. Introduction

Phytosterols, also known as plant sterols, are the main sterol fraction of plants, plant extracts, and vegetable oils. Phytosterols are analogs of cholesterol. Regarding their chemical structures, phytosterols are desmethylsterols, with a steroidal core composed of four carbon rings, three of them with six and one with five carbons. In this steroidal core, a hydroxyl group is found at third carbon, as well as double bonds can be found at the fifth or seventh carbon, differentiating the  $\Delta$ -5 from the  $\Delta$ -7 sterols, respectively. If there is no double bond, the sterol is saturated, and is commonly known as a stanol. The main difference

among all the sterol molecules is the side chain, attached to the twentieth carbon of the steroidal group. In this way, more than ten types of phytosterol molecules are naturally found (Fig. 1) (Fernandes & Cabral, 2007; Gómez-Coca, Pérez-Camino, & Moreda, 2015; Moreau, Whitaker, & Hicks, 2002).

Vegetable oils are composed of two main fractions namely, saponifiable and unsaponifiable. The saponifiable fraction is basically composed of triacylglycerols (TAG), three fatty acids bonded to a glycerol molecule. The fatty acids can be saturated or unsaturated. Palmitic (C 16:0) and stearic (C 18:0) acids are the main saturated fatty acids, while oleic (C 18:1) and linoleic (C 18:2) acids are the main

**Abbreviations:** FP, commercial food grade free phytosterol blend; SS, stigmasterol analytical standard; HOSO, high oleic sunflower oil; XRD, X-ray diffraction; RM, Rietveld method; CSD, Cambridge Structural Database;  $R_{wp}$ , Weighted Profile R-factor; PTO, pine tall oil; SODD, soybean oil deodorizer distillate; DSC, differential scanning calorimetry; GC, gas chromatograph; TAG, Triacylglycerol; SC, solid content;  $T_{co}$ , crystallization onset temperature;  $T_{mo}$ , melting onset temperature;  $T_{cp}$ , crystallization peak temperature;  $T_{mp}$ , melting peak temperature;  $\Delta H_c$ , crystallization enthalpie;  $\Delta H_m$ , melting enthalpie;  $T_{off c}$ , offset temperature of crystallization;  $T_{off m}$ , offset temperature of melting

\* Corresponding author.

E-mail address: [mayannygomes@hotmail.com](mailto:mayannygomes@hotmail.com) (M. Gomes Silva).

<https://doi.org/10.1016/j.foodres.2019.04.006>

Received 20 April 2018; Received in revised form 17 February 2019; Accepted 3 April 2019

Available online 04 April 2019

0963-9969/© 2019 Elsevier Ltd. All rights reserved.

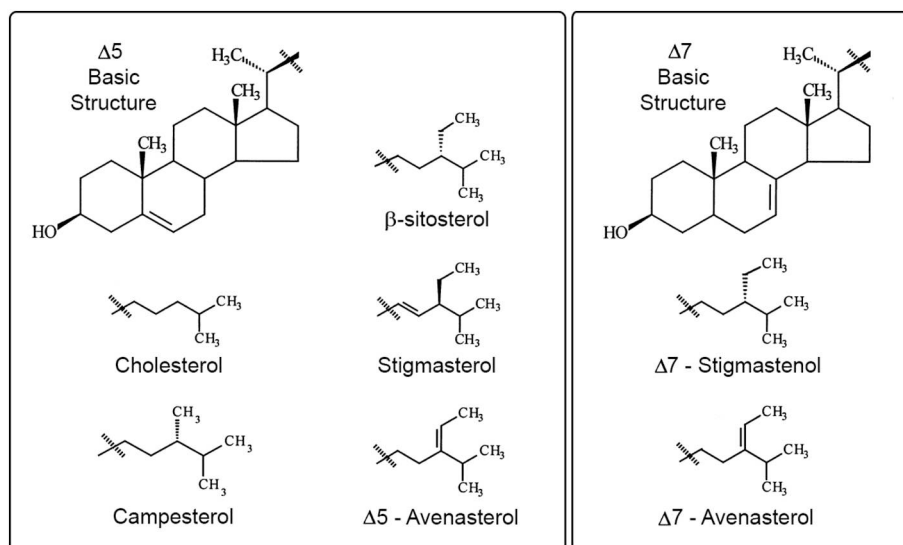


**Fig. 1.** Chemical structure of cholesterol and the main phytosterol according to their  $\Delta$ -5 and  $\Delta$ -7 basic structure. Adapted from Gómez-Coca, Pérez-Camino, & Moreda (2015).

unsaturated fatty acids found in vegetable oils. Phytosterols are present in the unsaponifiable fraction of plant lipids. The main phytosterols naturally found are  $\beta$ -sitosterol,  $\Delta$ -5 avenasterol, campesterol, and stigmasterol. The proportion of each sterol in the total sterol content, in other words, the phytosterol profile varies according to the plant source (Gómez-Coca et al., 2015). The main commercial sources of phytosterols are products of the vegetable oil industry, such as the soybean oil deodorizer distillate (SODD) and the waste residue of pine tall oil (PTO). Commercial phytosterols are indeed blends of phytosterols. Products from PTO are mainly composed of  $\beta$ -sitosterol +  $\Delta$ -5 avenasterol (~80%, due the quantification method for tall oil they are not commonly separated), with low amounts of campesterol (~7%), sitosterol, and campestanol, while products from SODD include  $\beta$ -sitosterol (~60%), campesterol (~25%), stigmasterol (20%), avenasterol, and others (Kumar, Mawlong, & Singh, 2017; Moreau, 2015; Ntanos, MacDougall, & Jones, 1998).

Regarding the consumption and bioactivity of phytosterols in humans, many studies have been carried out to demonstrate the beneficial effects of phytosterols in metabolism (Kritchevsky & Chen, 2005; Ostlund Jr, 2002). The first reported effect is the prevention of coronary disease. Due to their similarity to cholesterol, phytosterols are recognized for their ability to compete with cholesterol absorption resulting in the lowering of blood levels of cholesterol (Ling & Jones, 1995; Ntanos et al., 1998). Studies indicated that the consumption of 2 g of phytosterols per day had a significant effect on the reduction of cholesterol levels and consequently on coronary heart disease prevention (Moruise, Oosthuizen, & Opperman, 2006; Wu, Fu, Yang, Zhang, & Han, 2009). Recent studies have also indicated a strong association between phytosterol consumption and cancer prevention. A review article by Shahzad et al. (2017) reported that cancer prevention by the use of phytosterols is related to sterol biosynthesis modulation, improvement of the immune response and inhibition of tumor metastasis. Due to its biological activity, after the release of Benecol®, a spread enriched with phytosterols, in 1995, many food products have been developed using phytosterols and phytosterols as functional ingredients. In most cases, esterified phytosterols or stanols are used, mainly because of their low melting point and high solubility in the lipid phase (Fernandes & Cabral, 2007; Moreau, 2015). In recent years, based on the recommendation for the reduction of trans and saturated fatty acids in the diet (USDA, 2010), a new technology (non-triacylglycerol structuration) has been developed with the aim of structuring oils into a gel phase that can be used as a fat replacer in foods

(Chaves, Barrera-Arellano, & Ribeiro, 2017; Edmund Daniel Co and Marangoni, 2012). For this particular and new application, free phytosterols can be a good option when compared to esterified phytosterols, mainly because of their ability to self-assemble into stable crystal networks. However, few studies have been conducted for of this application of free phytosterol (Godoi et al., 2018; Sintang et al., 2017; Sintang et al., 2017; Yang et al., 2017; Yang, Chen, & Yang, 2017). Also, studies have reported that when free phytosterols are effectively heated and then recrystallized in fat upon cooling, they become bioavailable and therefore effective in reducing cholesterol absorption (Hayes, Pronczuk, & Perlman, 2004; Perlman, 2006). Moreover, although esterified phytosterols are easily incorporated into food products, they have unpredictable absorption rates, leading to variations in findings from human clinical trials (Clifton et al., 2004). This variation in absorption levels likely reflects the requirement to hydrolyze the esterified phytosterol before absorption. Phytosterol hydrolysis during digestion is subject to inter-individual variability, causing phytosterol absorption rates to vary between 40 and 96% (Carden et al., 2015; De Smet, Mensink, & Plat, 2012; Lubinus, Barnsteiner, Skurk, Hauner, & Engel, 2013). Thus, the application of free phytosterols in zero trans and low saturated lipid systems is very interesting, in addition to fulfilling the new nutritional recommendations and aggregate functionality to food products.

In this way, it is essential to understand the physical properties of phytosterols, mainly regarding the thermal phase transition and crystallization pattern. The events involved in  $\beta$ -sitosterol and stigmasterol crystallization have been described in physical blends with vegetable oils (Acevedo & Franchetti, 2016; Christiansen, Karjalainen, Seppänen-Laakso, Hiltunen, & Yliruusi, 2003; Daels, Foubert, & Goderis, 2017; Vaikousi, Lazaridou, Biliaderis, & Zawistowski, 2007; Zychowski et al., 2016), besides the interaction of these with cholesterol (Christiansen et al., 2003; Rozner, Popov, Uvarov, Aserin, & Garti, 2009). Pure phytosterols such as  $\beta$ -sitosterol and stigmasterol are characterized by high crystallinity, being able to form plate and needle-like crystals of anhydrous, hemi and monohydrates when crystallized in oil solutions or organic solvents (den Adel, Heussen, & Bot, 2010; Kawachi, Tanaka, Hirano, Igarashi, & Ooshima, 2006). They have a monoclinic unit cell, with small differences in unit cell parameters [*Stigmasterol hemihydrate*,  $C_{29}H_{48}O_{0.5} \cdot H_2O$ ,  $a = 9.367 \text{ \AA}$ ,  $b = 7.513 \text{ \AA}$ ,  $c = 36.857 \text{ \AA}$ ,  $\beta = 93.18^\circ$  (Benavides, Fronczek, & Fischer, 2002);  *$\beta$ -sitosterol monohydrate*,  $C_{29}H_{50}O \cdot H_2O$ ,  $a = 35.05 \text{ \AA}$ ,  $b = 7.550 \text{ \AA}$ ,  $c = 10.330 \text{ \AA}$ ,  $\beta = 92.0^\circ$  (Bernal, Crowfoot, & Fankuchen, 1940); and  *$\beta$ -sitosterol*

anhydro,  $C_{29}H_{50}O$ ,  $a = 38.05 \text{ \AA}$ ,  $b = 7.54 \text{ \AA}$ ,  $c = 9.74 \text{ \AA}$ , and  $\beta = 100.6^\circ$  (Moreno-Calvo et al., 2013)]. Thus, due to the high potential of the application of phytosterols as an oil structuring agent in foods, it is important to describe and understand the phase behavior phenomena involved in the crystallization of a phytosterol blend. To understand the thermal phase transition as well as the crystalline behavior in lipids systems, differential scanning calorimetry (DSC) and X-ray diffraction (XRD) are the key techniques. DSC provides exothermic and endothermic events during the thermal phase transition of crystallization and melting. It is also possible to understand the amount of energy released or absorbed during these events (Ribeiro, Basso, Grimaldi, Gioielli, & Gonçalves, 2009; Tan & Man, 2002). In lipids, the XRD profile is used to understand the subcell organization of the crystalline structures, providing the polymorphic behavior of triacylglycerols related to the  $\alpha$ ,  $\beta'$  and  $\beta$  forms (Ribeiro et al., 2009; Sonoda, Takata, Ueno, & Sato, 2004). Recently, Calligaris, da Silva, Ribeiro, dos Santos, and Cardoso (2018) have used XRD associated with the Rietveld structure refinement method (RM) to provide a quantitative analysis of triacylglycerol polymorphs. RM consists of carrying out least-squares iterations until the best fit is obtained between the observed power diffraction pattern and the calculated pattern (Rietveld, 1967; Young, 1993). This method enables the precise quantification of the crystalline phases that are present in a sample, and it is widely employed in many materials from distinct areas (Bish & Post, 1993; Guirado, Galí, & Chinchón, 2000; Németh, Sajó, & Demeter, 2010). The reliability of RM comes from the fact that the whole diffraction pattern contributes to the analysis; thus the impact of peak overlap and sample-related effects (such as preferred orientation) is minimized. Physical constants from crystal structure data are used for calculating reflection intensities and eliminating errors associated with intensity measurements and calibration procedures (McCusker, Von Dreele, Cox, Louër, & Scardi, 1999; Ruland, 1961). In this way, RM can further improve the quantitative approach to XRD results in free phytosterols in lipid systems with vegetable oil that are unprecedented in the literature (Acevedo & Franchetti, 2016; Christiansen, Rantanen, von Bonsdorff, Karjalainen, & Yliruusi, 2002; Daels et al., 2017; Sintang, Dona, et al., 2017; Vaikousi et al., 2007).

This study aims to investigate and compare the thermal phase transition and crystallization characteristics of a commercial food grade free phytosterol blend (FP) with a stigmaterol analytical standard (SS), as well as to understand the phase behavior during the addition of this phytosterol blend to high-oleic sunflower oil (HOSO) simulating the application in a food system. Here, the association of XRD and RM has been applied to the analysis of the FP:HOSO blends to obtain a quantitative analysis of the amorphous and crystalline content via RM, proposing a quantitative approach for the determination of phytosterol total content, using a physical instrumental method unprecedented in the literature.

## 2. Materials and methods

### 2.1. Raw materials

The materials used were high-oleic sunflower oil (HOSO) provided by Cargill Agrícola S/A® (Mairinque, SP, Brazil). Commercial food grade free phytosterol blend from tall oil (FP), was kindly offered by a national producer (under development) and the stigmaterol analytical standard (SS; 95%) was purchased from Sigma-Aldrich® (São Paulo, SP, Brazil). All other reagents and solvents were of analytical or chromatographic grades.

### 2.2. Fatty acid composition

The fatty acid composition of HOSO was determined in triplicate by gas chromatography (GC) with a capillary column-CGC Agilent 6850 Series GC System (Santa Clara, CA, USA), after esterification following

the method of Hartman and Lago (1973). The fatty acid methyl esters were separated according to the AOCS Ce 1f-96 method (AOCS, 2009) in a DB-23 Agilent capillary column (50% cyanopropyl methylpolysiloxane, length, 60 m, internal diameter, 0.25 mm and 0.25  $\mu\text{m}$  film thickness). The operating conditions were: oven temperature: 110 °C for 5 min, 110–215 °C (5 °C/min), 215 °C for 24 min; detector temperature: 280 °C; injector temperature: 250 °C; carrier gas: helium; split ratio: 1:50; injected volume: 1.0  $\mu\text{L}$ . The fatty acids were identified by comparison of the peak retention times with those of the respective fatty acid standards. The quantitative composition was calculated by area normalization expressed as the area percentage. The iodine and saponification values were determined according to AOCS methods Cd 1c-85 and Cd 3a-94 (AOCS, 2009).

### 2.3. Triacylglycerol composition (TAG)

The triacylglycerol composition of HOSO was determined by capillary gas chromatography with an Agilent 6850 Series GC System (Santa Clara, CA, USA) equipped with a capillary column DB-17 HT Agilent (50% phenyl-methylpolysiloxane; length, 15 m; internal diameter, 0.25 mm and 0.15  $\mu\text{m}$  film thickness). The operating conditions were: split, ratio of 1:100; column temperature: 250 °C, programmed to 340 °C at the rate of 5 °C/min; carrier gas: helium, at a flow rate of 1.0 mL/min; injector temperature: 360 °C, detector temperature: 375 °C; injected volume: 1.0  $\mu\text{L}$  and sample concentration 20 mg/mL of tetrahydrofuran. The identification of TAGs peaks was performed by comparison of the retention times, according to the procedure of Antoniosi Filho, Mendes, and Lanças (1995). The analysis was performed in triplicate.

### 2.4. Sterol composition

The identification and quantification of the major and minor sterol components of the FP were according to the AOCS Ce 12–16 method (AOCS, 2009). The sample was diluted in chloroform at a concentration of 1 mg/mL. Then, 0.5 mL of this solution was added to 0.5 mL of internal reference solution composed of 1 mg/mL  $\alpha$ -cholesterol in chloroform. The sample and internal reference were dried under nitrogen. After drying, the sample was derivatized with 500  $\mu\text{L}$  of a 1:3:9 (v/v/v) trimethylchlorosilane:hexamethyldisilazane:pyridine solution and analyzed by GC. The gas chromatograph Agilent 6850 Series GC System (Santa Clara, CA, USA) was equipped with an automated liquid sampler (1  $\mu\text{L}$  injections), split injector (1:50 split ratio), a fused silica low-polarity capillary column [Rxi-5HT (poly (5% diphenyl-95% dimethyl) siloxane; length, 30 m; intern diameter, 0.25 mm, and 0.25  $\mu\text{m}$  film thickness, Restek], and FID. The oven program for the determination of sterols was set isothermally at 265 °C. Helium was used as carrier gas at a flow rate of 1 mL/min. The temperatures of the injector and detector were 300 °C. The quantitative determination was done using the internal reference of  $\alpha$ -cholesterol. The data were expressed as the total percentage of sterols in the sample, by the ratio of the internal reference, and the percentage of the area of each sterol in the sample. Peak identification was performed by calculation of the retention time and comparison to the reference chromatograms.

### 2.5. Blend preparation

Blends of FP and HOSO in the proportions from 0 to 100% (w/w) of the FP in intervals of 10% were prepared after complete melting of the pure raw materials at 150 °C for 10 min to destroy the crystallinity memory under continuous stirring to ensure complete homogenization. For XRD and microstructure analysis, the blends were crystallized at 5 °C/24 h followed by crystalline stabilization at 25 °C/24 h. For the other analyses, the blends were stored at 25 °C until analysis. The FP and SS were analyzed without prior preparation.



## 2.6. Solid content (SC)

The solid content (SC) for FP:HOSO blends in triplicate was determined using the Nuclear Magnetic Resonance spectrometer Bruker pc120 Minispec (Rheinstetten, Germany) with a dry thermostatic bath with the temperature controlled by a Peltier System Tcon 2000, (Duratech, USA). The tempering procedures for non-stabilizing fats were performed according to the direct method recommended by American Oil Chemists' Society (AOCS, 2009), method Cd 16b-93, with modification of the maximum temperature to 140 °C, in triplicate. The term solid content was used without the term fat, as it relates to the evaluation of solids related to FP, which is not the common fat fraction (TAG).

## 2.7. Differential scanning calorimetry (DSC)

Thermal analyses of the SS, FP, and FP:HOSO blends were performed by differential scanning calorimetry (DSC), using a TA Thermal Analyzer, model Q2000 V4.7A, coupled to an RCS90 Refrigerated Cooling System (TA Instruments, Waters LLC, New Castle, USA). The thermal analyses were carried out under a dynamic atmosphere of N<sub>2</sub> (25 mL/min) in aluminum, with the reference being an empty capsule. Samples (6–12 mg) were subjected to the following temperature program: crystallization curves, 180 °C for 5 min, 180 °C to –80 °C (10 °C/min), and –80 °C for 30 min; and melting curves, –80 °C to 180 °C (5 °C/min). The TA Universal Analysis V4.7A software was used to obtain the curves and the following parameters: crystallization and melting onset temperatures ( $T_{co}$  and  $T_{mo}$ ), crystallization and melting peak temperatures ( $T_{cp}$  and  $T_{mp}$ ), crystallization and melting enthalpies ( $\Delta H_c$  and  $\Delta H_m$ ) and, offset temperature of crystallization and melting ( $T_{offc}$  and  $T_{offm}$ ) (Campos, 2005; Ribeiro, Basso, Grimaldi, Gioielli, & Gonçalves, 2009). All the DSC analyses were performed in triplicate.

### 2.7.1. Solubility behavior

The solubility behavior in the FP:HOSO blends was determined using the Hildebrand eq. (1) to describe the liquid-solid boundaries in the Pseudo-binary phase diagram of heating (Hildebrand, Prausnitz, & Scott, 1970; Höhne, Hemminger, & Flammersheim, 1996) as follows:

$$\frac{1}{T} - \frac{1}{T_0} = -\frac{R}{\Delta H} \ln X_2 \quad (1)$$

where  $T$  and  $T_0$  are the melting temperatures of the solid in solvent and in pure state, respectively;  $X_2$  is the molar fraction of the solid (FP);  $\Delta H$  is the heat of fusion of the solid and  $R$  is the universal gas constant. An average molecular weight of FP was assumed to be 413 g/mol, calculated using the phytosterol profile of FP, while that of HOSO was approximately 881 g/mol based on TAG composition. The melting temperatures of FP:HOSO blends were taken as the peak temperature of their melting endotherms.

## 2.8. X-ray diffraction (XRD) and Rietveld method (RM)

XRD analyses of the samples were performed at 25 °C using a Philips diffractometer (PW 1710) under the Bragg-Brentano geometry ( $\theta:2\theta$ ) with Cu-K $\alpha$  radiation ( $\lambda = 1.5418 \text{ \AA}$ , operating at 40 kV and 30 mA). Diffraction data were collected in the 5–40° range in  $2\theta$  with a 0.03° step scan and acquisition time of 3 s/step. All the XRD analyses were performed in triplicate.

In this work, the Rietveld method (RM) was applied to confirm the crystalline phase in the samples as well as to quantify their degree of crystallinity. This method consists of least-squares iterations until the best fit is obtained between the observed powder diffraction pattern and the calculated pattern based on the simultaneously refined models of the crystal structure, diffraction optics effects, instrumental factors, and other specimen characteristics (e.g., absorption and preferred orientation). In other words, RM optimizes the model function to

minimize the weighted sum of squared differences between the observed and calculated intensity values, i.e., to minimize  $\sum_i w_i (y_{Ci} - y_{Oi})^2$  where the weight, labeled as  $w_i$ , is  $1/\sigma^2[y_{Oi}]$ ,  $y_{Ci}$  and  $y_{Oi}$  are intensity values simulated from the model, where the  $C$  indicates are calculated and  $O$  are observed, and  $\sigma[y_{Oi}]$  is the standard uncertainty. Evaluation of the refinement can be performed using reliability factors (R-factors), generated during the adjustment. The most significant R-factor is  $R_{wp}$  (weighted profile R-factor) because the numerator of  $R_{wp}$  is the quantity that is actually minimized in the least-squares refinement procedure,  $R_{wp} = \sum_i w_i (y_{Ci} - y_{Oi})^2 / \sum_i w_i (y_{Oi})^2$ . The 0% value of  $R_{wp}$  represents an ideal fit, where a value of 10% is acceptable for most cases. Another R-factor is the  $R_{exp}$  (expected R-factor), which is defined as best value that can be reached by  $R_{wp}$ , considering the initial model. The ratio of these values defines another useful statistical parameter known as  $GOF$  (Goodness of Fit) and  $\chi^2$ , according to the equation  $[GOF]^2 = [\chi^2] = [R_{wp}/R_{exp}]^2$ . A  $GOF$  value of 1.0 indicates that the refinement is complete, that is, the best statistical value for the refinement was obtained. In addition to the above agreement indices, the reliability of the refinement must be checked on the basis of final structure and lattice parameters. Occupation factors and thermal displacement parameters need to be physically meaningful values and interatomic distances and bond angles should be reasonable from a crystal-chemical point of view (Izumi, 1996; Toby, 2006; Young, 1993).

To confirm the crystalline phase in the samples, the whole pattern fits were done using the Fundamental Parameters approach available on TOPAS analytical software version 4.2 (Bruker AXS) (Coelho, Evans, Evans, Kern, & Parsons, 2011; McCusker et al., 1999). The calculated pattern used was that for  $\beta$ -sitosterol, obtained from the Crystallographic Information Files (.cif) available via CSD (Cambridge Structural Database) v5.39 (Moreno-Calvo et al., 2013). This analysis was done by allowing some structural parameters to vary in a limited range (restraints) from its original values to ensure that the bonds between the atoms forming the crystalline structure are maintained, even after refinement. The employed restrictions were as follows: a) lattice parameters – allowed to differ from the original structures by 5% at maximum; b) carbon (C) and oxygen (O) atomic positions – variation up to 0.02 Å in all three lattice unit vector directions; and c) hydrogen atomic positions were kept constrained to their closest carbon and oxygen neighbors, i.e., the positions were linked to the C and O.

## 2.9. Degree of crystallinity

The TOPAS analytical software, version 4.2 (Bruker AXS) was used for providing the quantitative analysis of crystalline and amorphous phase in samples, and thus, to quantify the FP content in the blends. In this approach, the whole XRD pattern is fit by RM, where the crystalline content of the sample is responsible for any sharp XRD peak and the amorphous content and incoherent scattering contribute to the smooth background (Ruland, 1961; Vonk, 1973). In the present work, a split pseudo-Voigt (SPV) function was applied to fit the broad background signal from the amorphous phase with a peak inserted at  $2\theta \sim 18.5^\circ$ , while the background followed a 3rd order polynomial Chebyshev function. The crystalline function was described by a  $\beta$ -sitosterol structure obtained from the Crystallographic Information Files (.cif) available via CSD (Cambridge Structural Database) v5.39 (Moreno-Calvo et al., 2013). Therefore, crystalline and amorphous concentrations were obtained by their related intensity areas over the whole pattern intensity area (Calligaris et al., 2018; Madsen, Scarlett, & Kern, 2011).

## 2.10. Crystalline size

The crystallite size ( $D$ ) to the FP:HOSO blends was determined using the Scherrer eq. (2) (Holzwarth & Gibson, 2011; Klug & Alexander, 1974) as follows:

$$D = K \lambda / \beta_{hkl} \theta \quad (2)$$

where,  $K$  is the Scherrer constant or shape factor, 0.89 (as the shape of the crystallite is unknown);  $\lambda$  is the  $\text{CuK}\alpha$  wavelength of 1.5418 Å;  $\beta_{hkl}$  is the full width at half maximum ( $FWHM$ ) of the diffraction peak in radians; and  $\theta$  is the Braggs diffraction angle. The estimation and comparison of the average crystallite size were carried out by using the peak at  $14.9^\circ 2\theta$  (011) contribution at the XRD measures. This peak was selected because of the highest intensity among all reflections and not overlapped with adjacent reflections.

### 2.11. Microstructure

Crystalline morphology was evaluated at  $25^\circ\text{C}$  using polarized light microscopy (Olympus, model BX 51, San Jose, USA) coupled to a digital video camera (Media Cybernetics, model MicroPublisher 5.0 Mpixel, Bethesda, USA). The images were captured by the applicative cell Sens Standard version 1.7.1 (Olympus Corporation, San Jose, EUA), using polarized light under a magnification of  $\times 10$ . Duplicate slides were prepared for each sample within each slide and three visual fields were arbitrarily chosen and focused (Campos, 2005).

### 2.12. Statistic

DSC e XRD data were statistically analyzed using the Statistical System version 12 software (SAS Institute Inc., USA). To determine significant differences between the mean values of the tests, an analysis of variance (ANOVA), followed by Tukey's test was applied at a level of  $p < .05$ .

## 3. Results and discussion

### 3.1. Chemical composition of raw materials

The fatty acid composition is the main characterization analysis for fats and oils. Regular sunflower oil is composed mainly of linoleic acid (C18:2), while in HOSO, the oleic acid (C18:1) is predominant. The changes in fatty acid profiles from regular sunflower oil to HOSO improve the oxidative stability of the oil, highlighting HOSO as an important raw material for the development of stable foods. The fatty acid profile (area %), iodine and saponification calculated values from the HOSO sample are shown in Table 1. The predominant unsaturated fatty acids in HOSO were oleic acid (C18:1, 78.60%) and linoleic acid (C18:2, 11.41%). Additionally, saturated fatty acids, such as palmitic (C16:0, 4.31%), stearic (C18:0, 3.16%) and behenic (C22:0, 0.88%) acids were also detected. These results are in agreement with those found in the literature (Codex Alimentarius, 1999).

The triacylglycerol composition refers to the distribution of fatty acids into the molecules of TAG, an important parameter related to the physical behavior during thermal phase transitions of fats and oils. The chemical configurations of TAGs play an important role in the packing form of TAGs during crystallization. In Table 1 is shown that the predominant TAG species in HOSO were OOO (~65%), followed by OLO (~15%), POO (~11.2%), and OLL/PLO (~3%). This composition is very homogeneous when compared to other vegetable oils and can be used easily in lipid model systems.

Regarding the chemical composition of FP, two analyses were performed, the phytosterol profile and the purity degree of the blend. The main phytosterols were  $\beta$ -sitosterol and  $\Delta$ -5-avenasterol, ~73 and 18%, respectively. In addition, 6.25% campesterol, 1.67% campestanol, and 0.35% stigmasterol were also detected. Based on the phytosterol profile, it is possible to deduce the origin of the phytosterols. Therefore, the FP sample comes from tall oil, since phytosterols from SODD contain more campesterol and stigmasterol.

The chemical composition of raw materials is very important to

**Table 1**

Chemical composition of raw materials HOSO and FP. Fatty acid (%), iodine value ( $\text{g I}_2 / 100 \text{ g}$ ), saponification value ( $\text{mg KOH/g}$ ) and triacylglycerol composition (%) from HOSO, phytosterol profile and purity of FP.

High Oleic Sunflower Oil		
Fatty acid composition		
Fatty acids		Area % <sup>a</sup>
C16:0 - palmitic acid		4.31 ± 0.71
C18:0 - stearic acid		3.16 ± 0.42
C18:1 - oleic acid		78.60 ± 2.94
C18:2 - linoleic acid		11.41 ± 1.06
C22:0 - behenic acid		0.88 ± 0.03
Σ saturated <sup>b</sup>		9.32
Σ unsaturated <sup>b</sup>		90.68
I. V.		88.34
S. V.		190.59
Triacylglycerol composition		
CN	TAG	Area %
52	POSt	0.84 ± 0.40
	POO	10.04 ± 0.40
	PLO	2.93 ± 0.44
	StOO	2.03 ± 1.23
54	OOO	65.95 ± 1.74
	OLO	15.34 ± 0.59
	OLL	2.87 ± 0.23
Commercial food grade free phytosterol blend		
Phytosterol profile		
Phytosterols		Area % <sup>c</sup>
Campesterol		6.25 ± 0.11
Campestanol		1.67 ± 0.02
Stigmasterol		0.35 ± 0.01
β-sitosterol		73.39 ± 0.24
Δ-5-avenasterol		18.34 ± 0.35
Purity of phytosterols		
Phytosterols (% w/w) <sup>c</sup>		99.38 ± 1.05

CN – Carbon number; P = palmitic acid; St = stearic acid; O = oleic acid; L = linoleic acid;

I. V. iodine value ( $\text{g I}_2 / 100 \text{ g}$ ), S. V. saponification value calculated ( $\text{mg KOH/g}$ ).

<sup>a</sup> Values are the means of triplicate determination ± standard deviation. Values below 0.5% were excluded from the table.

<sup>b</sup> Calculated from the mean of fatty acid composition, thus, no standard deviation was showed.

<sup>c</sup> Mean of three replicates ± Standard Deviation.

understand the physical behavior of the blends. The crystallization of a vegetable oil/fat is dependent of the fatty acids and triacylglycerol composition, mainly when blended with other lipid sources such as FP. Thus, this composition is essential to understand the HOSO interference in the FP crystallization when they were blended. As will be further discussed, due to the fatty acid composition, HOSO is not crystalline in our conditions interfering with the solubility and dilution of FP crystals.

### 3.2. Solid content (SC)

The solid fraction, relative to the whole mass as a function of temperature, indicates basic physico-chemical and structural attributes of the lipid system. Furthermore, the SC is useful in formulating and developing new products (Danthine and Deroanne, 2006). SC values for the investigated FP:HOSO blends are given in Fig. 2. The SC of the blends was directly proportional to the addition of FP to HOSO at all evaluated temperatures. The higher the amount of FP the higher the melting point of the blend. This behavior indicates that the only solid fraction in the blends was from FP, as well as an interaction between HOSO and FP to lower the melting point of the blend. Possibly due to the presence of HOSO, FP crystals became less organized and packaged, facilitating the energy transfer to the system due to the FP melting.

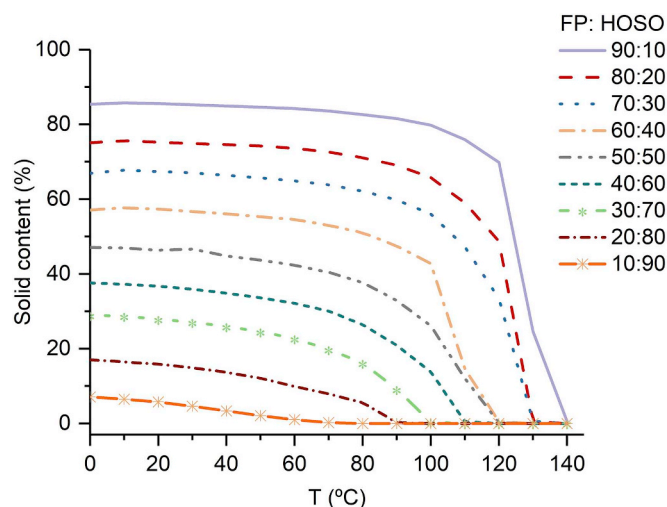


Fig. 2. Solid content (%) (SC) as a function of the temperature of phytosterol and high oleic sunflower oil blends (FP: HOSO) in the proportions of the FP from 10 to 90% (w/w) in intervals of 10%.

When analyzing the SC parameter used for food applications, it is essential to take into account the food processing temperatures to reach the melting point of the blend and proper dispersion of the components into the food product.

### 3.3. Differential scanning calorimetry (DSC)

The melting and crystallization behavior of SS, FP, and FP:HOSO blends is shown in Fig. 3. The crystallization and melting parameters derived from the thermal curves are shown in Tables 2 and 3, respectively. The selected parameters include: onset temperature of crystallization ( $T_{co}$ ) and melting ( $T_{mo}$ ), which refers to the start of the thermal phase transition; peak temperature of crystallization ( $T_{cp}$ ) and melting ( $T_{mp}$ ), wherein the thermal effect is maximum; enthalpy of crystallization ( $\Delta H_c$ ) and melting ( $\Delta H_m$ ) or thermal phase transition enthalpy, measured by the area under/over the curve; and offset temperature of crystallization ( $T_{off_c}$ ) and melting ( $T_{off_m}$ ), which indicates the termination of the thermal effect (Campos, 2005; Ribeiro, Basso, Grimaldi, Gioielli, & Gonçalves, 2009).

A single crystallization peak was observed for SS and FP (Fig. 3-a) with the maximum crystallization temperatures for SS and FP at 127.44 °C and 122.91 °C, respectively. The  $T_{co}$  and  $T_{off_c}$  were 126.83 and 93.90 °C for the SS and 124.17 and 110.13 °C for the FP. These results show that the start of the thermal phase transition and the conclusion of the thermal effect were similar for both samples, indicating that phytosterols had crystallization behaviors similar to SS, even when in an FP. A single peak was verified for the melting temperature (Fig. 3-b) of both samples that was higher for SS (169.14 °C) than FP (135.87 °C). The enthalpy in the exothermic events (64.16 and 36.75 J/g) and the endothermic events (58.74 and 24.71 J/g) were determined. As expected for pure compounds, these results demonstrate that the SS releases more energy to a thermal phase transition in the crystallization events as well as in the melting, compared to the blend (FP). These results are consistent with the literature. Vaikousi et al. (2007) found that sterol from soybean oil (purity of 86.2% - composed of 36.8% of  $\beta$ -sitosterol, 23.5% of campesterol, 23.1% of stigmasterol and 2.8% of brassicasterol), melted at 139.48 °C and showed an enthalpy of melting of 40.86 J/g. This similar behavior from SS and FP support the technique of crystallization studies of phytosterols using FP in HOSO. Besides, the blends are a real system, viable to food applications.

The thermal behavior of FP:HOSO blends produced two characteristic peaks, the first related to FP fraction (peak 1) and the second to

HOSO (peak 2). Peak 1 diminished, and peak 2 increased in intensity with increasing HOSO content in the blends. As shown in Fig. 3-c, with increasing oil content, the crystallization peaks of FP decreased and moved to lower temperatures than 100% of the FP. Only a single crystallization peak was observed in the phytosterol-oil blends with incorporation up to 70% of FP (FP:HOSO - 90:10, 80:20 and 70:30), showing  $T_{cp}$  at 114.97, 106.09 and 107.37 °C, respectively. These narrow peaks indicated that the blend of FP crystallization in the HOSO is uniform. In addition, the  $T_{cp}$  found in this concentration range is very similar to the 100% of FP crystallization behavior. However, the FP incorporation of 60 to 30% in to HOSO showed in two clear crystallization peaks. The first (peak 1-  $T_{cp}$  1) was related to FP crystallization, from 100 to 87 °C, and the second peak (peak 2-  $T_{cp}$  2) to the crystallization of the HOSO (−56 to −58 °C). For the blends FP:HOSO (20:80) and FP:HOSO (10:90), the  $T_{cp}$  1 was observed at 32.61 and −39.06 °C (as a shoulder), respectively, and can be seen more clearly in Fig. 3-e. These events may be related to the dispersion effect of FP into HOSO that changes the solubility equilibrium of the system or nonuniform crystallization of the system. Both change the thermal events that are observed in the DSC analysis. The melting behavior of the FP:HOSO blends were similar to crystallization behavior. The  $T_{mp}$  1 associated with FP became broader and moved to lower temperatures with increasing HOSO (Fig. 3-d).  $T_{mp}$  1 shifted from 135.87 to 81.32 °C, until the concentration of 20% of HOSO, where  $T_{mp}$  1 is observed. For FP:HOSO (10:90), only  $T_{mp}$  2 associated with HOSO was observed. Similar melting behavior was reported for different free phytosterols in corn oil by Vaikousi et al. (2007), who attributed this behavior to the solubility effects of oil. These solubility effects are also related to the reduction in enthalpy of both the crystallization and melting peaks.

Pseudo-binary phase diagram for FP:HOSO blends composed with the offset and onset temperatures of melting is shown in Fig. 4-a. Although the thermal protocol used in this study (constant heating rate) did not produce equilibrium states, the ensuing kinetic binary phase diagram allows analysis of the solubility of the two materials and may be extrapolated to describe equilibrium states (Bouziadi & Narine, 2012; Daels et al., 2017). In the diagram, the top line (V- open triangle) indicates the complete melting temperature of the system. Above this line all the system is liquid. On the other hand, the bottom line (● - closed circle) is related to the solid line, indicating the total crystallization of the system, and below this line, the system is crystallized solid. Two different regions can be seen on the diagram, one related to HOSO between, the ● - closed circle and ○ - open circle, and the second associated with FP, between the ▼ - closed triangle and V- open triangle. These regions are known a metastable region, where the liquid and solid fractions of HOSO and/or FP are concomitantly present. Indirectly, these regions represent the solubility of HOSO and FP in the system according to the temperature. When liquid, the component is considered soluble; when solid, it is insoluble. Less variation was noticed in the HOSO metastable region with the increase in HOSO concentration in the system; however, the metastable region of FP varies with the proportion of FP in the system. The melting temperature increases with an increased concentration of FP in the system. The FP fraction starts and ends the melting phase transition at a higher temperature with the increase in FP in the system. In this way, the metastable zone can be modulated through the modification of the concentration of FP in the system. In other words, the solubility of FP in a lipid food system can be modified according to the concentration of FP in the food system, as well as the food process can be adjusted to reach the complete solubility of the components. Fig. 4-b reveals linear relationships between the DSC melting temperature and the molar fraction of FP in HOSO (estimated  $R^2$  value was 0.97) in fairly good agreement with Eq. 1. The enthalpy of melting, 23.15 J/g for FP calculated from the respective slopes is similar to the DSC experimental value of  $24.08 \pm 0.94$  J/g for FP. This approach, in general, allows the prediction of the behavior of added lipid phases of FP in processed foods, where solubility effects are paramount.

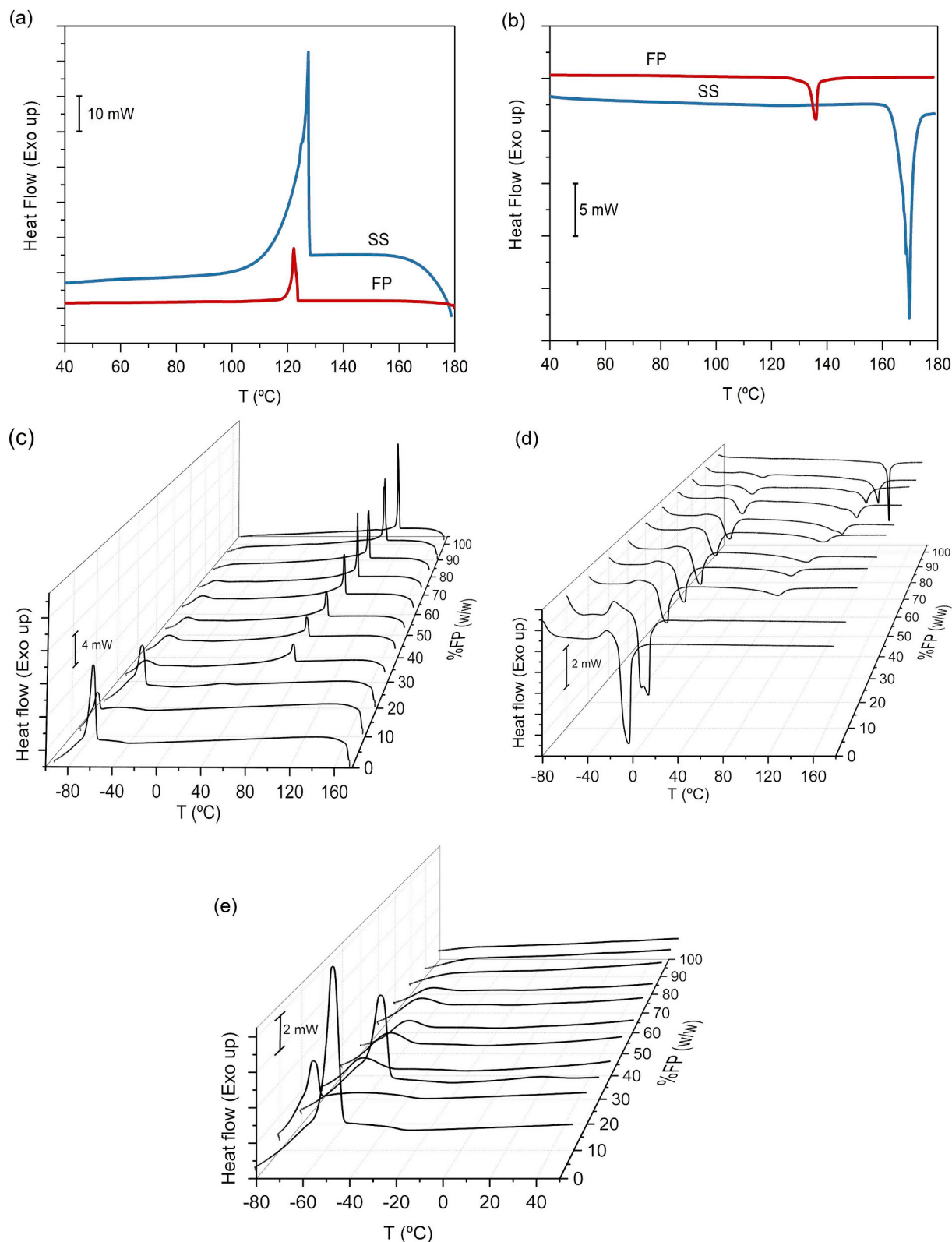


**Fig. 3.** (a) Crystallization and (b) melting curves of the FP and SS. (c) Crystallization and (d) melting curves for FP: HOSO blends in the proportions of FP from 0 to 100% (w/w) in intervals of 10%. (e) Detail for the crystallization curve of FP:HOSO blends in the temperature range  $-80$  and  $50^{\circ}\text{C}$ .

### 3.4. X-ray diffraction and crystallinity analysis

Diffraction patterns for SS, FP and its blends with HOSO measured at  $25^{\circ}\text{C}$  are shown in Fig. 5. The main peaks corresponding to the diffraction spacing are also summarized in Table 4. The FP shows a

pattern for pure  $\beta$ -sitosterol similar to that reported in the literature (Acevedo & Franchetti, 2016; Christiansen et al., 2002). Although FP is a blend of several phytosterols,  $\beta$ -sitosterol is the major component, as verified GC analysis data, which explains the observed behavior. The crystallographic information from the literature for  $\beta$ -sitosterol was



**Table 2**

Crystallization onset temperatures ( $T_{co}$ ), crystallization peak temperatures ( $T_{cp}$ ), crystallization enthalpies ( $\Delta H_c$ ) and offset temperature of crystallization ( $T_{offc}$ ) of the stigmasterol (SS), commercial food grade free phytosterol blend (FP) and phytosterols-oil blends (FP:HOSO).

Samples	Peak 1 (FP)				Peak 2 (HOSO)			
	$T_{co}$ (°C) 1	$T_{cp}$ (°C) 1	$T_{offc}$ (°C) 1	$\Delta H_c$ (J/g) 1	$T_{co}$ (°C) 2	$T_{cp}$ (°C) 2	$T_{offc}$ (°C) 2	$\Delta H_c$ (J/g) 2
SS	126.83 ± 1.15 <sup>a</sup>	127.44 ± 0.02 <sup>a</sup>	93.90 ± 0.26 <sup>b</sup>	64.16 ± 2.28 <sup>a</sup>	–	–	–	–
FP:HOSO (% w/w)								
100:0	124.17 ± 0.94 <sup>b</sup>	122.91 ± 0.65 <sup>b</sup>	110.13 ± 0.13 <sup>a</sup>	36.75 ± 0.88 <sup>b</sup>	–	–	–	–
90:10	116.98 ± 0.46 <sup>c</sup>	114.97 ± 0.80 <sup>c</sup>	88.51 ± 0.42 <sup>c</sup>	31.18 ± 0.82 <sup>c</sup>	–	–	–	–
80:20	107.94 ± 0.01 <sup>d</sup>	106.09 ± 1.07 <sup>d</sup>	85.64 ± 0.16 <sup>d</sup>	28.80 ± 0.56 <sup>c</sup>	–	–	–	–
70:30	108.63 ± 0.41 <sup>d</sup>	107.37 ± 0.05 <sup>d</sup>	77.54 ± 0.53 <sup>c</sup>	28.81 ± 0.09 <sup>c</sup>	–	–	–	–
60:40	102.12 ± 0.85 <sup>e</sup>	100.83 ± 0.91 <sup>e</sup>	72.08 ± 0.40 <sup>f</sup>	18.94 ± 1.28 <sup>d</sup>	–46.47 ± 0.07 <sup>c</sup>	–58.63 ± 0.91 <sup>d</sup>	–65.79 ± 0.27 <sup>b</sup>	5.09 ± 0.34 <sup>d</sup>
50:50	96.81 ± 0.69 <sup>f</sup>	94.95 ± 0.61 <sup>f</sup>	65.02 ± 0.27 <sup>g</sup>	19.41 ± 0.22 <sup>d</sup>	–45.91 ± 0.31 <sup>c</sup>	–56.60 ± 0.57 <sup>c</sup>	–66.19 ± 0.13 <sup>b</sup>	6.01 ± 0.97 <sup>d</sup>
40:60	88.87 ± 0.57 <sup>g</sup>	86.44 ± 0.16 <sup>g</sup>	61.43 ± 0.14 <sup>h</sup>	13.96 ± 1.40 <sup>e</sup>	–46.05 ± 0.46 <sup>c</sup>	–56.77 ± 0.93 <sup>c</sup>	–65.65 ± 0.40 <sup>b</sup>	6.93 ± 0.35 <sup>d</sup>
30:70	89.30 ± 0.21 <sup>h</sup>	86.40 ± 0.87 <sup>g</sup>	58.26 ± 0.70 <sup>i</sup>	14.22 ± 0.91 <sup>e</sup>	–48.72 ± 0.39 <sup>d</sup>	–60.77 ± 0.19 <sup>c</sup>	–66.33 ± 0.42 <sup>b</sup>	7.60 ± 0.16 <sup>d</sup>
20:80	44.79 ± 0.05 <sup>h</sup>	32.61 ± 0.01 <sup>h</sup>	–2.20 ± 0.86 <sup>j</sup>	2.37 ± 0.03 <sup>f</sup>	–40.05 ± 0.29 <sup>a</sup>	–44.44 ± 0.27 <sup>a</sup>	–60.87 ± 0.58 <sup>a</sup>	24.77 ± 0.57 <sup>b</sup>
10:90	–18.46 ± 0.77 <sup>i</sup>	–39.06 ± 0.77 <sup>i</sup>	–60.47 ± 0.01 <sup>i</sup>	3.63 ± 0.64 <sup>f</sup>	–61.71 ± 0.18 <sup>e</sup>	–65.13 ± 0.29 <sup>f</sup>	–70.05 ± 0.80 <sup>c</sup>	–14.71 ± 1.22 <sup>c</sup>
0:100	–	–	–	–	–40.92 ± 0.16 <sup>b</sup>	–46.43 ± 0.81 <sup>b</sup>	–59.21 ± 1.08 <sup>a</sup>	34.34 ± 2.11 <sup>a</sup>

Values are shown as mean ± standard deviation of three replications. Means with different letters within the column indicate that the samples are statistically different ( $p < .05$ ) by Tukey's test.

used in the RM to confirm the crystalline phase for the FP (Fig. 5-a). XRD Rietveld method analysis confirms that FP crystallizes in a monoclinic structure (space group -  $P2_1$ ). The refined pattern ( $I_{cal}$ ) shows a good concordance with the experimental data ( $I_{obs}$ ) and the obtained R factor was  $R_{wp} = 10.06 \pm 0.26\%$ . The values  $a = 37.79 \pm 0.21 \text{ \AA}$ ,  $b = 7.52 \pm 0.02 \text{ \AA}$ ,  $c = 9.69 \pm 0.08 \text{ \AA}$ ,  $\beta = 100.36 \pm 0.09^\circ$ , and  $V = 2784.24 \pm 71.71 \text{ \AA}^3$  obtained by the Rietveld analysis for the compound lattice parameters agree with those reported in the literature for  $\beta$ -sitosterol (Moreno-Calvo et al., 2013). For SS, the RM (Fig. 5-b) also showed good agreement between  $I_{obs}$  and  $I_{cal}$ , with  $R_{wp}$  of  $13.70\% \pm 0.03$ , with the lattice parameters  $a = 10.11 \pm 0.11$ ,  $b = 6.86 \pm 0.09$ ,  $c = 32.53 \pm 0.32$  and  $\beta = 94.50 \pm 0.32^\circ$  also showing a good agreement with those reported in the literature for these compound (Pettit et al., 2003). The similarity between the diffraction pattern of FP with pure phytosterols,  $\beta$ -sitosterol, reported in the literature, is a positive characteristic for FP. As the FP is composed of several phytosterols, its application in foods is more feasible when compared to analytical grade compounds.

All the FP:HOSO blends (Fig. 5-c) had an XRD pattern similar to FP. However, an increase in heightened background intensity in the angular range  $12\text{--}25^\circ$  ( $2\theta$ ) with increasing HOSO concentration in the blends is observed. Such behavior is expected because the HOSO is liquid at room temperature, thus contributing to the amorphous content in XRD pattern for the blends. In XRD analyses the long spacing and

short spacing peaks provide information about the order and the lateral packing of the molecular layers, respectively. For FP:HOSO blends was observed that short and long spacing peaks showed higher intensity with increments of HOSO. This suggested that the increase of vegetable oil to FP caused changes in the physical state of samples, which become more fluid, contributing to change the intensity of the observed XRD reflections (Sagiri, Singh, Pal, Banerjee, & Basak, 2015). This behavior was associated with the dispersion effect of HOSO, and similar results were observed in microstructure analysis. Retention of peaks in the long spacing region revealed that the order of the FP molecular layers was not disturbed, even in the blends. The peak d-spacing of  $\sim 37 \text{ \AA}$  for the samples corresponds to the organization in a double layer (whereas a  $\beta$ -sitosterol molecule of approximately  $18\text{--}22 \text{ \AA}$ ), and the peak at  $\sim 18 \text{ \AA}$  corresponds to the length of FP molecules (Acevedo & Franchetti, 2016; Bot, den Adel, & Roijers, 2008; Moreno-Calvo et al., 2013; Sagiri et al., 2015; Yang, Li, et al., 2017). To verify the incorporation of the HOSO within the layers of FP molecules, the average crystallite size ( $D$ ) was analyzed using the Scherrer equation (Eq. 2) (Holzwarth & Gibson, 2011; Klug & Alexander, 1974). The addition of HOSO in to FP resulted in distinct variation in the crystallite sizes in the blends, as shown in Table 5. The crystallite size increased with the increase of HOSO in the blends, from  $74.152 \pm 1.130 \text{ nm}$  in FP:HOSO (90:10) to  $114.674 \pm 2.174 \text{ nm}$  in FP:HOSO (50:50). This change to larger crystallite sizes indicates that the spaces between the grains of the crystals

**Table 3**

Melting onset temperatures ( $T_{mo}$ ), melting peak temperatures ( $T_{mp}$ ), melting enthalpies ( $\Delta H_m$ ) and offset temperature of melting ( $T_{offm}$ ) of the stigmasterol (SS), commercial food grade free phytosterol blend (FP) phytosterols-oil blends (FP:HOSO).

Samples	Peak 1 (FP)				Peak 2 (HOSO)			
	$T_{mo}$ (°C) 1	$T_{mp}$ (°C) 1	$T_{offm}$ (°C) 1	$\Delta H_m$ (J/g) 1	$T_{mo}$ (°C) 2	$T_{mp}$ (°C) 2	$T_{offm}$ (°C) 2	$\Delta H_m$ (J/g) 2
SS	165.42 ± 0.02 <sup>a</sup>	169.14 ± 0.02 <sup>a</sup>	174.05 ± 0.68 <sup>a</sup>	–58.74 ± 1.92 <sup>c</sup>	–	–	–	–
FP:HOSO (% w/w)								
100:0	133.26 ± 0.16 <sup>b</sup>	135.87 ± 0.15 <sup>b</sup>	144.47 ± 0.59 <sup>c</sup>	–24.71 ± 0.94 <sup>d</sup>	–	–	–	–
90:10	125.90 ± 0.93 <sup>c</sup>	132.34 ± 0.38 <sup>c</sup>	147.04 ± 0.85 <sup>b</sup>	–19.55 ± 0.73 <sup>c</sup>	–23.77 ± 0.03 <sup>f</sup>	–10.48 ± 0.02 <sup>e</sup>	2.05 ± 0.36 <sup>e</sup>	–6.00 ± 0.85 <sup>a</sup>
80:20	118.73 ± 0.41 <sup>d</sup>	127.81 ± 0.52 <sup>d</sup>	143.25 ± 0.86 <sup>cd</sup>	–19.48 ± 0.55 <sup>c</sup>	–21.74 ± 0.31 <sup>e</sup>	–8.86 ± 0.11 <sup>d</sup>	6.05 ± 1.20 <sup>d</sup>	–12.15 ± 0.38 <sup>b</sup>
70:30	109.06 ± 0.71 <sup>e</sup>	123.05 ± 1.91 <sup>e</sup>	142.45 ± 0.55 <sup>d</sup>	–25.86 ± 0.70 <sup>d</sup>	–18.49 ± 0.49 <sup>d</sup>	–7.73 ± 0.19 <sup>c</sup>	9.43 ± 0.31 <sup>c</sup>	–20.77 ± 0.18 <sup>c</sup>
60:40	108.16 ± 0.97 <sup>e</sup>	120.61 ± 0.34 <sup>f</sup>	135.17 ± 0.86 <sup>e</sup>	–19.70 ± 0.93 <sup>c</sup>	–16.58 ± 0.25 <sup>c</sup>	–5.32 ± 0.34 <sup>b</sup>	11.34 ± 0.40 <sup>bc</sup>	–26.88 ± 0.50 <sup>d</sup>
50:50	85.65 ± 0.34 <sup>f</sup>	110.35 ± 0.01 <sup>g</sup>	126.96 ± 0.66 <sup>f</sup>	–12.12 ± 0.05 <sup>b</sup>	–16.83 ± 0.04 <sup>c</sup>	–5.48 ± 0.12 <sup>b</sup>	14.94 ± 0.54 <sup>a</sup>	–31.27 ± 0.91 <sup>e</sup>
40:60	80.61 ± 0.04 <sup>h</sup>	106.49 ± 0.85 <sup>h</sup>	119.77 ± 0.14 <sup>g</sup>	–11.41 ± 0.27 <sup>b</sup>	–16.84 ± 0.28 <sup>c</sup>	–5.26 ± 0.18 <sup>b</sup>	13.07 ± 0.27 <sup>ab</sup>	–34.41 ± 0.24 <sup>f</sup>
30:70	82.93 ± 0.99 <sup>g</sup>	101.91 ± 0.19 <sup>j</sup>	121.70 ± 0.87 <sup>g</sup>	–10.70 ± 0.04 <sup>b</sup>	–15.58 ± 0.28 <sup>b</sup>	–4.90 ± 0.35 <sup>b</sup>	14.67 ± 0.60 <sup>a</sup>	–37.27 ± 0.51 <sup>g</sup>
20:80	67.77 ± 0.87 <sup>i</sup>	81.32 ± 0.91 <sup>j</sup>	91.13 ± 0.27 <sup>h</sup>	–1.25 ± 0.36 <sup>a</sup>	–15.33 ± 0.24 <sup>b</sup>	–4.84 ± 0.32 <sup>b</sup>	11.16 ± 0.75 <sup>bc</sup>	–36.64 ± 0.21 <sup>h</sup>
10:90	–	–	–	–	–15.16 ± 0.10 <sup>b</sup>	–4.78 ± 0.44 <sup>b</sup>	13.03 ± 1.95 <sup>b</sup>	–48.70 ± 0.96 <sup>h</sup>
0:100	–	–	–	–	–13.84 ± 0.53 <sup>a</sup>	–3.82 ± 0.14 <sup>a</sup>	11.07 ± 1.31 <sup>bc</sup>	–58.72 ± 0.96 <sup>i</sup>

Values are shown as mean ± standard deviation of three replications. Means with different letters within the column indicate that the samples are statistically different ( $p < .05$ ) by Tukey's test.

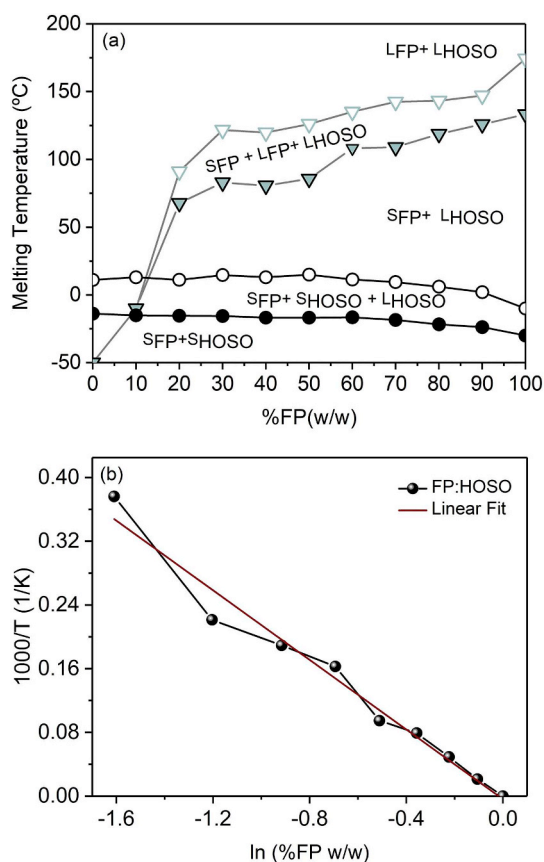


**Fig. 4.** (a) Pseudo-Diagram for FP:HOSO blends composed with the offset and onset temperatures of melting; S - solid; L - liquid. (b) Melting temperatures of FP:HOSO blends as a function of the molar fraction of FP in HOSO according to Eq. 1.

(each grain in a polycrystalline aggregate) have been altered, associated with a larger separation between the grains. This behavior might be associated with the incorporation of HOSO into the system. For concentrations of HOSO > 50% (w/w), a reduction in crystallite size was observed. Such behavior is associated with amorphization (dispersion effect) of the system. The crystallite size calculation for FP:HOSO (10:90) and FP:HOSO (20:80) samples could not be performed due to a large amorphous fraction, making it difficult to calculate accurately. The amorphization of systems is already well known to cause a reduction in crystallite size (Gusain, Srivastava, Singh, & Sharma, 2014; Niu & Hampshire, 2002; Sagiri et al., 2015). These crystallite sizes are in concordance with those observed by RM.

RM was applied to the FP:HOSO blends to quantify the crystalline and amorphous phases by weight. The addition of a Split Pseudo-Voigt peak (SPV) to represent the substantial increase in amorphous content was able to describe the overall background together with a smooth 3rd order polynomial Chebyshev function. In Fig. 6, it is possible to see the contribution from the SPV (amorphous) for FP:HOSO blends and the crystalline phase well-described the observed XRD peaks during the RM. By comparing the relative intensity areas from crystalline and amorphous phases, one can confirm that with the increase in HOSO concentration, the profile is mainly ruled by the amorphous peak, although still presenting FP peaks. The results obtained for the crystalline and amorphous weight phase in the FP:HOSO blends with corresponding  $R_{wp}$  values obtained by RM are shown in Table 6. The quantitative results are expected to reflect the same experimental mass ratio of the blends, and the good agreement with the expected concentrations are clearly observed with the use of RM. It would be difficult to achieve such results only by evaluating peak intensity, mainly if the concentration of each component in the blend is not known. In this way, the application of RM in FP:HOSO blends to quantify the crystalline and amorphous phases can be useful for an initial determination of the phytosterol content present in vegetable oil. For a physical method, XRD is less expensive, less laborious and much faster compared to the conventional analytical methods currently used to quantify total phytosterols, which use various organic solvents in different analytical steps. It is worthwhile to mention that in the present work, the minimum concentration of phytosterol used was 10% in vegetable oil. Therefore,

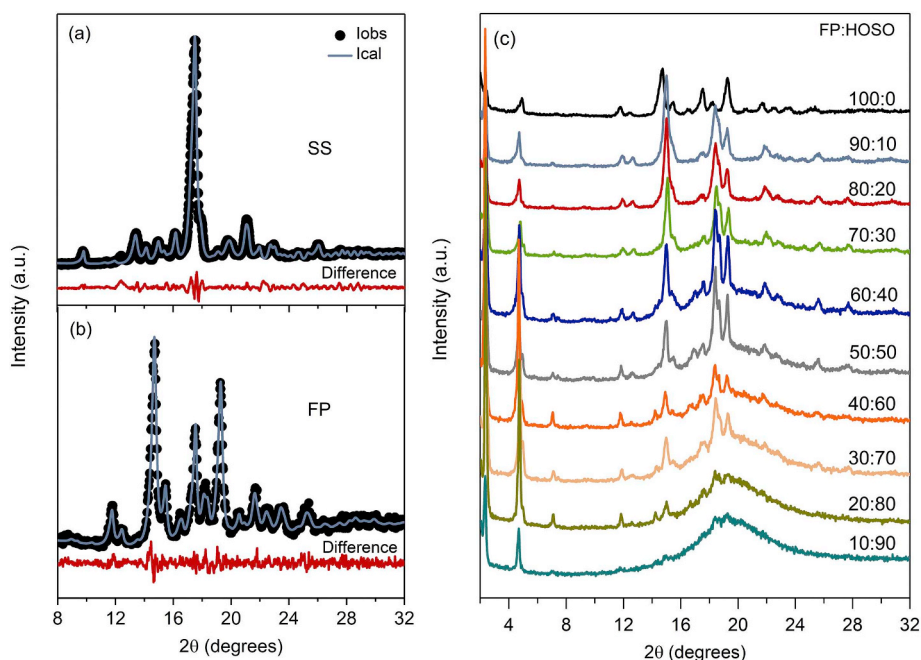


**Fig. 5.** (a) Rietveld results for stigmasterol (SS) and (b) commercial food grade free phytosterol blend (FP). (c) XRD patterns of the pure commercial phytosterol (FP) and its blends with HOSO.

**Table 4**  
Main peaks corresponding to the diffraction line spacing for FP, SS and FP:HOSO blends.

Sample	Long Spacing		Short spacing	
	Peak position (2 $\theta$ )	d-spacing (Å)	Peak position (2 $\theta$ )	d-spacing (Å)
FP	2.57; 4.77; 5.07; 7.53	36.48; 18.53; 17.44; 11.74	11.37; 12.68; 13.78; 14.95; 15.59; 16.70; 17.73; 18.43; 18.79; 19.42; 21.59; 21.92; 22.85; 23.46; 25.09; 25.61; 27.80; 30.98;	7.39; 6.98; 6.43; 5.93; 5.68; 5.31; 5.00; 4.82; 4.72; 4.57; 4.12; 4.05; 3.89; 3.79; 3.55; 3.50; 3.21; 2.89
SS	2.42; 4.76; 5.04; 7.53	36.46; 18.54; 17.54; 11.74	11.35; 12.29; 13.41; 14.93; 15.51; 16.16; 17.50; 17.91; 18.43; 18.90; 19.63; 21.03; 21.84; 22.87; 23.46; 24.59; 27.55; 29.28	7.79; 7.19; 6.60; 5.93; 5.71; 5.48; 5.07; 4.95; 4.82; 4.69; 4.52; 4.22; 4.07; 3.89; 3.55; 3.62; 3.24; 3.04
FP:HOSO (% w/w)				
90:10	2.38; 4.73; 5.07; 7.04;	37.24; 18.68; 17.44; 12.55;	11.86; 12.62; 13.78; 15.03; 15.48; 16.70; 17.59; 18.41; 18.70; 19.27; 21.17; 21.89; 22.96; 23.66; 25.43; 25.62; 27.79; 30.72	7.46; 7.02; 6.43; 5.89; 5.72; 5.31; 5.10; 4.82; 4.74; 4.61; 4.19; 4.06; 3.87; 3.76; 3.50; 3.48; 3.21; 2.91
80:20	2.38; 4.74; 5.07; 7.05	37.09; 18.65; 17.44; 12.54	11.92; 12.69; 13.78; 15.01; 15.48; 16.70; 17.52; 18.41; 18.69; 19.28; 21.17; 21.87; 22.69; 23.66; 25.59; 25.62; 27.68; 30.72	7.42; 6.97; 6.43; 5.90; 5.72; 5.31; 5.06; 4.82; 4.74; 4.60; 4.19; 4.06; 3.92; 3.76; 3.50; 3.48; 3.22; 2.91
70:30	2.46; 4.80; 5.07; 7.14	35.91; 18.40; 17.44; 12.38	11.95; 12.74; 13.78; 15.09; 15.48; 16.70; 17.59; 18.46; 18.78; 19.35; 21.17; 21.92 22.88; 23.66; 25.62; 25.71; 27.71; 30.72	7.41; 6.95; 6.43; 5.87; 5.72; 5.31; 5.04; 4.80; 4.72; 4.59; 4.19; 4.05; 3.89; 3.76; 3.50; 3.46; 3.22; 2.91
60:40	2.39; 4.74; 5.07; 7.12	36.91; 18.64; 17.44; 12.41	11.87; 12.68; 13.78; 15.01; 15.48; 16.97; 17.59; 18.41; 18.73; 19.31; 21.17; 21.88; 22.73; 23.66; 25.62; 25.63; 27.68; 30.72	7.45; 6.98; 6.43; 5.90; 5.72; 5.22; 5.04; 4.82; 4.74; 4.59; 4.19; 4.06; 3.91; 3.76; 3.50; 3.48; 3.22; 2.91
50:50	2.36; 4.71; 5.07; 7.05	37.45; 18.77; 17.44; 12.53	11.85; 12.64; 13.78; 15.02; 15.47; 16.93; 17.59; 18.40; 18.69; 19.26; 21.17; 21.79; 22.75; 23.66; 25.62; 25.59; 27.80; 30.72	7.47; 7.00; 6.43; 5.89; 5.73; 5.24; 5.04; 4.82; 4.74; 4.61; 4.19; 4.08; 3.91; 3.76; 3.50; 3.48; 3.21; 2.91
40:60	2.35; 4.69; 5.07; 7.05	37.58; 18.82; 17.44; 12.54	11.80; 12.55; 13.78; 14.20; 14.94; 15.48; 16.61; 17.58; 18.38; 18.64; 19.23; 21.17; 21.77; 23.66; 25.45; 25.62; 27.80; 30.72	7.49; 7.05; 6.43; 6.24; 5.93; 5.72; 5.34; 5.04; 4.83; 4.76; 4.61; 4.19; 4.082; 3.76; 3.50; 3.48; 3.21; 2.91
30:70	2.41; 4.76; 5.07; 7.11	36.69; 18.58; 17.44; 12.43	11.89; 12.68; 13.78; 14.28; 15.01; 15.48; 16.70; 17.67; 18.41; 19.29; 21.17; 21.90; 22.79; 23.66; 25.62; 25.67; 27.76; 30.72	7.44; 6.98; 6.43; 6.20; 5.90; 5.72; 5.31; 5.02; 4.82; 4.59; 4.19; 4.06; 3.90; 3.76; 3.50; 3.47; 3.21; 2.91
20:80	2.38; 4.74; 5.07; 7.09	37.08; 18.66; 17.44; 12.47	11.84; 14.22; 15.04; 16.58; 17.59; 18.37; 19.33	7.47; 6.23; 5.88; 5.35; 5.04; 4.83; 4.59
10:90	2.35; 4.69; 5.07; 7.05	37.58; 18.84; 17.44; 12.53	11.75; 14.93; 18.38; 19.22	7.53; 5.93; 4.83; 4.62

**Table 5**  
The XRD parameters and crystallite size of SS, FP and FP:HOSO blends.

Sample	d-spacing of [011] plane (Å)	FWHM of [011] peak (°2θ)	D (nm)
SS	5.934 ± 0.001 <sup>a</sup>	0.237 ± 0.001 <sup>d</sup>	87.797 ± 0.217 <sup>d</sup>
FP	5.928 ± 0.002 <sup>a</sup>	0.296 ± 0.001 <sup>b</sup>	71.649 ± 0.366 <sup>e</sup>
FP:HOSO (% w/w)			
90:10	5.928 ± 0.001 <sup>a</sup>	0.325 ± 0.002 <sup>a</sup>	74.152 ± 1.130 <sup>e</sup>
80:20	5.900 ± 0.008 <sup>ab</sup>	0.208 ± 0.002 <sup>c</sup>	110.574 ± 1.749 <sup>bc</sup>
70:30	5.869 ± 0.001 <sup>b</sup>	0.178 ± 0.003 <sup>f</sup>	145.840 ± 0.824 <sup>a</sup>
60:40	5.901 ± 0.002 <sup>ab</sup>	0.207 ± 0.002 <sup>c</sup>	114.317 ± 2.870 <sup>b</sup>
50:50	5.895 ± 0.004 <sup>ab</sup>	0.204 ± 0.002 <sup>c</sup>	114.674 ± 2.174 <sup>b</sup>
40:60	5.929 ± 0.001 <sup>a</sup>	0.206 ± 0.003 <sup>c</sup>	104.802 ± 2.792 <sup>c</sup>
30:70	5.902 ± 0.002 <sup>ab</sup>	0.266 ± 0.004 <sup>c</sup>	87.062 ± 0.538 <sup>d</sup>
20:80	–	–	–
10:90	–	–	–

Values are shown as mean ± standard deviation of three replications. Means with different letters within the column indicate that the samples are statistically different ( $p < .05$ ) by Tukey's test.

additional studies required to determine the minimum detectable concentration of phytosterol in oil by XRD will be part of a forthcoming paper, since RM can provide quantitative information even for traces of analyte.

### 3.5. Crystal morphology

Fig. 7 shows the microstructure of FP:HOSO blends obtained by polarized light microscopy. The HOSO (liquid oil) is optically isotropic and appeared to be dark, whereas FP crystals appear as bright areas. The microstructure of pure FP (Fig. 7-a) consisted of aggregated spherulites, similar to previous research on phytosterols (Acevedo & Franchetti, 2016; Sintang, Dona, et al., 2017; Yang, Li, et al., 2017). The spherulites were formed through the aggregation of needle-like crystals,

**Table 6**  
Crystalline and amorphous weight phase in the FP:HOSO blends with related  $R_{wp}$  values obtained by Rietveld method.

FP:HOSO (% w/w)	Crystalline (wt%)	Amorphous (wt%)	$R_{wp}$ (%)
90:10	89.57 ± 0.27 <sup>a</sup>	10.43 ± 0.27 <sup>i</sup>	8.13 ± 0.16 <sup>de</sup>
80:20	79.45 ± 0.37 <sup>b</sup>	20.55 ± 0.30 <sup>h</sup>	8.10 ± 0.04 <sup>de</sup>
70:30	70.34 ± 0.17 <sup>c</sup>	29.66 ± 0.98 <sup>g</sup>	10.86 ± 1.64 <sup>ab</sup>
60:40	60.07 ± 0.12 <sup>d</sup>	39.93 ± 0.12 <sup>f</sup>	8.96 ± 0.12 <sup>bcd</sup>
50:50	50.70 ± 0.38 <sup>e</sup>	49.30 ± 0.38 <sup>e</sup>	8.71 ± 0.63 <sup>cd</sup>
40:60	39.51 ± 0.25 <sup>f</sup>	60.49 ± 0.25 <sup>d</sup>	10.61 ± 0.40 <sup>abc</sup>
30:70	31.63 ± 0.38 <sup>g</sup>	68.37 ± 0.38 <sup>c</sup>	10.81 ± 0.05 <sup>abc</sup>
20:80	20.88 ± 0.30 <sup>h</sup>	79.12 ± 0.30 <sup>b</sup>	12.38 ± 0.27 <sup>a</sup>
10:90	10.27 ± 0.17 <sup>i</sup>	89.73 ± 0.17 <sup>a</sup>	6.07 ± 0.06 <sup>e</sup>

Values are shown as mean ± standard deviation of three replications. Means with different letters within the column indicate that the samples are statistically different ( $p < .05$ ) by Tukey's test.

grown from a nucleation center and had several orders of branching, thus forming large crystal structures. This type of morphology has been associated with the ability of FP to structure liquid lipid phases. As seen from the images, the incorporation of HOSO caused a reduction in the large agglomeration of FP crystals and dispersion of crystalline aggregates (spherulites) of FP crystals. For the blends with the highest concentration of HOSO, FP:HOSO (20:80) and FP:HOSO (10:90) (Fig. 7-i and j), the crystals were more elongated, with lower density aggregates. These results are attributed to the dilution effect of the HOSO in the blends, agreeing with the DSC and XRD analysis. Sintang, Dona, et al. (2017) and Sintang, Danthine, et al. (2017), while investigating the oil structuring in monoacylglycerols and phytosterol blends observed that the needle-shaped or mixed crystals resulted in better network formation, with no oil exudation or crystalline phase precipitation over several months of storage. Thus, FP:HOSO blends with higher concentrations of HOSO appear to be more suitable for applications when stability is allowed.

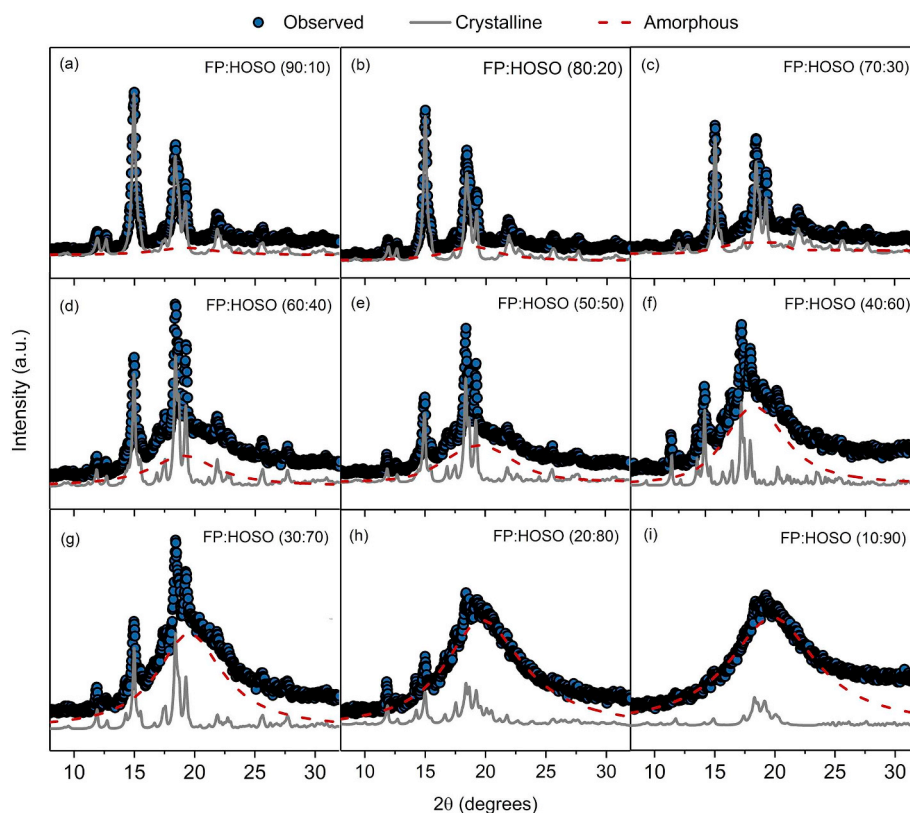


**Fig. 6.** Distinguishing between the crystalline and amorphous portions using the Rietveld method for FP:HOSO blends.



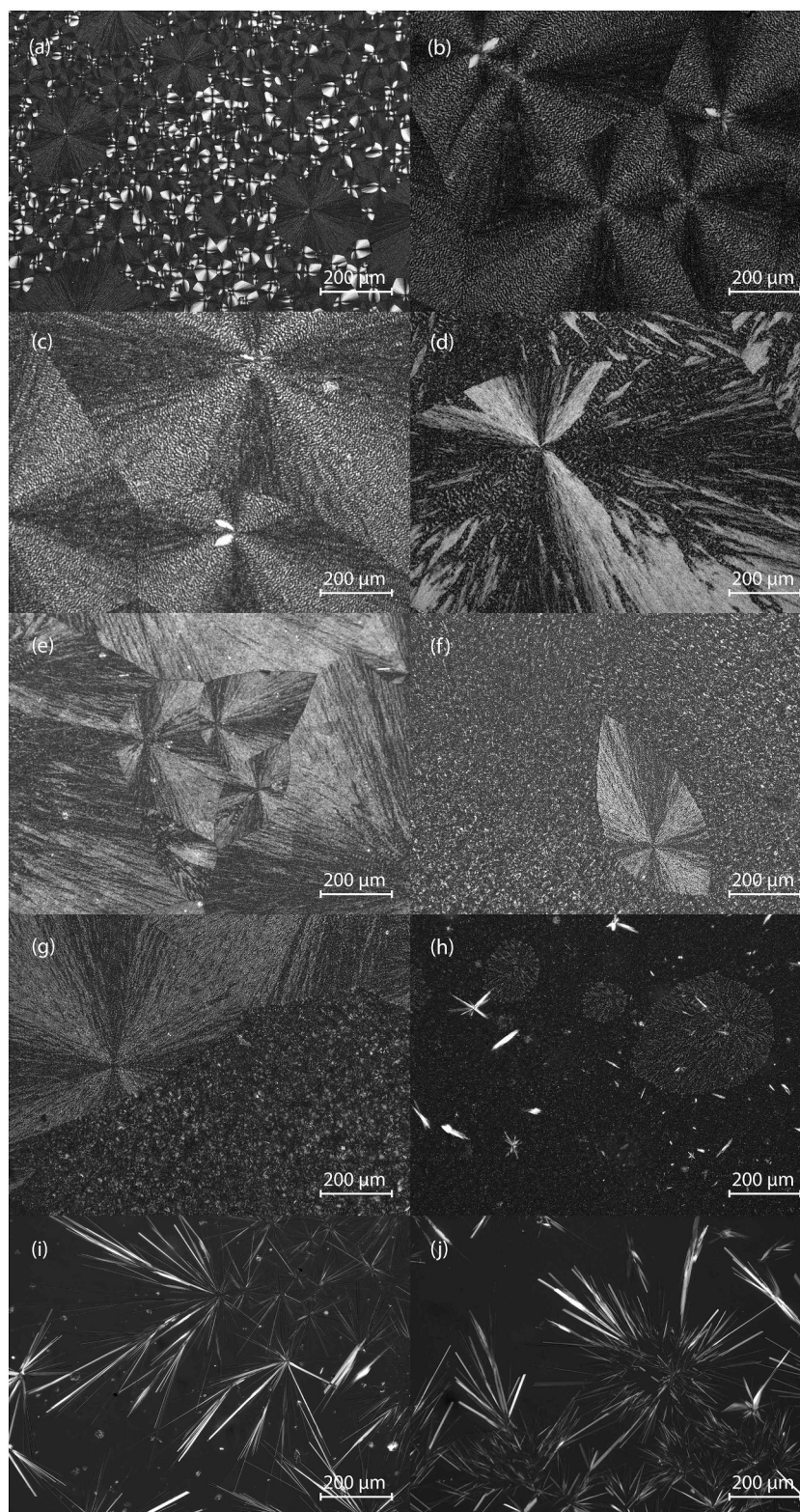


**Fig. 7.** Microstructure of the crystals with magnification of  $10\times$ : obtained by a) FP; b) FP:HOSO (90:10); c) FP:HOSO (80:20); d) FP:HOSO (70:30); e) FP:HOSO (60:40); f) FP:HOSO (50:50); g) FP:HOSO (40:60); h) FP:HOSO (30:70); i) FP:HOSO (20:80) and j) FP:HOSO (10:90).

#### 4. Conclusion

In summary, we have studied the thermal phase transitions, as well as crystal characteristics, XRD pattern, crystallinity, and morphology, of FP, SS, and FP:HOSO blends using several analytical techniques. The FP, although composed of a mixture of several phytosterols, showed

thermal behavior and X-ray diffraction patterns similar to pure phytosterols ( $\beta$ -sitosterol and stigmasterol). Thus, mixtures of phytosterols may be an inexpensive alternative compared to pure compounds for applications in the food industry. The dispersion effect was mainly responsible for the thermal and crystalline behavior observed in the FP:HOSO blends. The thermal behavior of FP:HOSO blends showed two

characteristic peaks, the first related to the FP fraction and the second to HOSO. With the increase of the oil content, the crystallization peaks of FP decreased and shifted to lower temperatures than 100% of the FP. Dispersion effects were also observed in the solid content, with a reduction in the melting point of the blends with the increase HOSO content. The microstructure of pure FP consisted of aggregated spherulites. The incorporation of HOSO caused a reduction in the large agglomeration of FP crystals and disintegration of crystalline aggregates of FP crystals. In the XRD pattern of the blends the dispersion effect of HOSO in the FP was observed by an increase in the amorphous fraction. This behavior was explored to apply the Rietveld method to quantify the amorphous and crystalline fraction present in the blends, and was applied successfully. Hence, the results of our study made it possible to investigate and to understand FP loaded HOSO systems. Also, the study considers a physical method for an initial determination of the phytosterol content of vegetable oils using the Rietveld method, that is unprecedented in the literature.

## Acknowledgments

The authors thank the Brazilian funding agencies CNPq and FAPESP [grant number 16/11261-8], for the financial support of this work. This study was financed in part by the “Coordenação de Aperfeiçoamento de Pessoal de Nível Superior - Brazil (CAPES)”- Finance Code 001.

## References

- Acevedo, N. C., & Franchetti, D. (2016). Analysis of co-crystallized free phytosterols with triacylglycerols as a functional food ingredient. *Food Research International*, 85, 104–112.
- Alimentarius, C. (1999). Codex standard for named vegetable oils. *Codex Stan*, 210, 1–13.
- Antoniosi Filho, N., Mendes, O., & Lanças, F. (1995). Computer prediction of triacylglycerol composition of vegetable oils by HPLC. *Chromatographia*, 40(9–10), 557–562.
- AOCS (2009). *Official Methods and Recommended Practices of the AOCS*. Champaign: AOCS Press.
- Benavides, G. A., Fronczek, F. R., & Fischer, N. H. (2002). Stigmasterol hemihydrate. *Acta Crystallographica Section C*, 58(3), o131–o132.
- Bernal, J. D., Crowfoot, D., & Fankuchen, I. (1940). X-ray crystallography and the chemistry of the steroids. Part I. *Philosophical Transactions of the Royal Society London A*, 239(802), 135–182.
- Bish, D. L., & Post, J. E. (1993). Quantitative mineralogical analysis using the Rietveld full-pattern fitting method. *American Mineralogist*, 78(9–10), 932–940.
- Bot, A., den Adel, R., & Roijers, E. C. (2008). Fibrils of  $\gamma$ -oryzanol +  $\beta$ -sitosterol in edible oil organogels. *Journal of the American Oil Chemists' Society*, 85(12), 1127–1134.
- Bouzidi, L., & Narine, S. S. (2012). Relationships between molecular structure and kinetic and thermodynamic controls in lipid systems: Part III. Crystallization and phase behavior of 1-palmitoyl-2, 3-stearyl-sn-glycerol (PSS) and tristearoylglycerol (SSS) binary system. *Chemistry and Physics of Lipids*, 165(1), 105–119.
- Calligaris, G. A., da Silva, T. L., Ribeiro, A. P. B., dos Santos, A. O., & Cardoso, L. P. (2018). On the quantitative phase analysis and amorphous content of triacylglycerols materials by X-ray Rietveld method. *Chemistry and Physics of Lipids*, 212, 51–60.
- Campos, R. (2005). Experimental methodology. *Fat crystal networks*, 267–349.
- Carden, Trevor J., et al. (2015). Dietary plant sterol esters must be hydrolyzed to reduce intestinal cholesterol absorption in hamsters. *J. Nutr.* 145(7), 1402–1407.
- Chaves, K. F., Barrera-Arellano, D., & Ribeiro, A. P. B. (2017). Potential application of lipid organogels for food industry. *Food Research International*, 105, 863–872.
- Christiansen, L., Karjalainen, M., Seppänen-Laakso, T., Hiltunen, R., & Yliruusi, J. (2003). Effect of  $\beta$ -sitosterol on precipitation of cholesterol from non-aqueous and aqueous solutions. *International Journal of Pharmaceutics*, 254(2), 155–166.
- Christiansen, L. I., Rantanen, J. T., von Bonsdorff, A. K., Karjalainen, M. A., & Yliruusi, J. K. (2002). A novel method of producing a microcrystalline  $\beta$ -sitosterol suspension in oil. *European Journal of Pharmaceutical Sciences*, 15(3), 261–269.
- Clifton, P. M., Noakes, M., Ross, D., Fassoulakis, A., Cehun, M., & Nestel, P. (2004). High dietary intake of phytosterol esters decreases carotenoids and increases plasma plant sterol levels with no additional cholesterol lowering. *Journal of Lipid Research*, 45(8), 1493–1499.
- Coelho, A. A., Evans, J., Evans, I., Kern, A., & Parsons, S. (2011). The TOPAS symbolic computation system. *Powder Diffraction*, 26(SupplementS1), S22–S25.
- Dael, E., Foubert, I., & Goderis, B. (2017). The effect of adding a commercial phytosterol ester mixture on the phase behavior of palm oil. *Food Research International*, 100, 841–849.
- Braipson-Danthine, Sabine, & Deroanne, Claude (2006). Determination of solid fat content (SFC) of binary fat blends and use of these data to predict SFC of selected ternary fat blends containing low-eruc rapeseed oil. *J. Am. Oil Chem. Soc.* 83(7), 571–581.
- De Smet, E., Mensink, R. P., & Plat, J. (2012). Effects of plant sterols and stanols on intestinal cholesterol metabolism: Suggested mechanisms from past to present. *Molecular Nutrition & Food Research*, 56(7), 1058–1072.
- den Adel, R., Heussen, P. C., & Bot, A. (2010). Effect of water on self-assembled tubules in  $\beta$ -sitosterol +  $\gamma$ -oryzanol-based organogels. *Paper Presented at the Journal of Physics: Conference Series*.
- Edmund Daniel Co, & Marangoni, A. G. (2012). Organogels: An alternative edible oil-structuring method. *Journal of the American Oil Chemists' Society*, 89(5), 749–780.
- Fernandes, P., & Cabral, J. (2007). Phytosterols: Applications and recovery methods. *Bioresource Technology*, 98(12), 2335–2350.
- Godoi, K., Basso, R., Buscato, M., Cardoso, L., Kieckbusch, T., & Ribeiro, A. (2018). Dispersed free phytosterols as structuring agents in lipid systems with reduced saturated fat. *Grasas y Aceites*, 68(4), 217.
- Gómez-Coca, R., Pérez-Camino, M., & Moreda, W. (2015). Neutral lipids: Unsaponifiable. *Handbook of Food Analysis*, 22, 459–489.
- Guirado, F., Galí, S., & Chinchón, S. (2000). Quantitative Rietveld analysis of aluminous cement clinker phases. *Cement and Concrete Research*, 30(7), 1023–1029.
- Gusain, D., Srivastava, V., Singh, V. K., & Sharma, Y. C. (2014). Crystallite size and phase transition demeanor of ceramic steel. *Materials Chemistry and Physics*, 145(3), 320–326.
- Hartman, L., & Lago, R. C. (1973). Rapid preparation of fatty acid methyl esters from lipids. *Laboratory Practices*, 22, 475–476.
- Hayes, K., Pronczuk, A., & Perlman, D. (2004). Nonesterified phytosterols dissolved and recrystallized in oil reduce plasma cholesterol in gerbils and humans. *The Journal of Nutrition*, 134(6), 1395–1399.
- Hildebrand, J. H., Prausnitz, J. M., & Scott, R. L. (1970). *Regular and Related Solutions: The Solubility of Gases, Liquids, and Solids*. Van Nostrand Reinhold Co.
- Höhne, G. W. H., Hemminger, W., & Flammersheim, H.-J. (1996). Theoretical fundamentals of differential scanning calorimeters. *Differential scanning Calorimetry* (pp. 21–40). Springer.
- Holzwarth, U., & Gibson, N. (2011). The Scherrer equation versus the Debye-Scherrer equation. *Nature Nanotechnology*, 6(9), 534.
- Izumi, F. (1996). The Rietveld method and its applications to synchrotron X-ray powder data. *Analytical Spectroscopy Library. Vol. 7. Analytical Spectroscopy Library* (pp. 405–452). Elsevier.
- Kawachi, H., Tanaka, R., Hirano, M., Igarashi, K., & Ooshima, H. (2006). Crystallization of  $\beta$ -sitosterol using a water-immiscible solvent hexane. *Journal of Chemical Engineering of Japan*, 39(8), 869–875.
- Klug, H. P., & Alexander, L. E. (1974). X-ray diffraction procedures: For polycrystalline and amorphous materials. X-ray diffraction procedures: For polycrystalline and amorphous materials, 2nd Edition, By Harold P. Klug, Leroy E. Alexander, (pp. 992). ISBN 0-471-49369-4. Wiley-VCH, (May 1974).
- Kritchevsky, D., & Chen, S. C. (2005). Phytosterols—Health benefits and potential concerns: A review. *Nutrition Research*, 25(5), 413–428.
- Kumar, S., Mawlong, I., & Singh, D. (2017). Phytosterol recovery from oilseeds: Recent advances. *Journal of Food Process Engineering*, 40(3).
- Ling, W., & Jones, P. (1995). Dietary phytosterols: A review of metabolism, benefits and side effects. *Life Sciences*, 57(3), 195–206.
- Lubinus, T., Barnsteiner, A., Skurk, T., Hauner, H., & Engel, K.-H. (2013). Fate of dietary phytosteryl/–stanol esters: Analysis of individual intact esters in human feces. *European Journal of Nutrition*, 52(3), 997–1013.
- Madsen, I., Scarlett, N., & Kern, A. (2011). Description and survey of methodologies for the determination of amorphous content via X-ray powder diffraction. *Zeitschrift für Kristallographie Crystalline Materials*, 226(12), 944–955.
- McCusker, L., Von Dreele, R., Cox, D., Louër, D., & Scardi, P. (1999). Rietveld refinement guidelines. *Journal of Applied Crystallography*, 32(1), 36–50.
- Moreau, R. A. (2015). Composition of plant sterols and stanols in supplemented food products. *Journal of AOAC International*, 98(3), 685–690.
- Moreau, R. A., Whitaker, B. D., & Hicks, K. B. (2002). Phytosterols, phytostanols, and their conjugates in foods: Structural diversity, quantitative analysis, and health-promoting uses. *Progress in Lipid Research*, 41(6), 457–500.
- Moreno-Calvo, E., Temelli, F., Cordoba, A., Masciocchi, N., Veciana, J., & Ventosa, N. (2013). A new microcrystalline phytosterol polymorph generated using CO<sub>2</sub>-expanded solvents. *Crystal Growth & Design*, 14(1), 58–68.
- Morui, K. G., Oosthuizen, W., & Opperman, A. M. (2006). Phytosterols/stanols lower cholesterol concentrations in familial hypercholesterolemic subjects: A systematic review with meta-analysis. *Journal of the American College of Nutrition*, 25(1), 41–48.
- Német, Z., Sajó, I., & Demeter, Á. (2010). Rietveld refinement in the routine quantitative analysis of famotidine polymorphs. *Journal of Pharmaceutical and Biomedical Analysis*, 51(3), 572–576.
- Niu, H., & Hampshire, D. (2002). Fabrication of nanocrystalline and amorphous Chevrel phase PbMo<sub>6</sub>S<sub>8</sub> powder by ball milling. *Physica C: Superconductivity*, 372, 1145–1147.
- Ntanios, F. Y., MacDougall, D. E., & Jones, P. J. (1998). Gender effects of tall oil versus soybean phytosterols as cholesterol-lowering agents in hamsters. *Canadian Journal of Physiology and Pharmacology*, 76(7–8), 780–787.
- Ostlund, R. E., Jr. (2002). Phytosterols in human nutrition. *Annual Review of Nutrition*, 22(1), 533–549.
- Perlman, D., Hayes, K., & Pronczuk, A. (2006). *Prepared foods containing triglyceride-crystallized non-esterified phytosterols*. (U.S. Patent No. 7,144,595).
- Pettit, G. R., Meng, Y., Herald, D. L., Graham, K. A., Pettit, R. K., & Doubek, D. L. (2003). Isolation and structure of Ruprechtsteryl from Ruprechtia tangarana<sup>a</sup>, 1. *Journal of Natural Products*, 66(8), 1065–1069.
- Ribeiro, A. P. B., Basso, R. C., Grimaldi, R., Gioielli, L. A., dos Santos, A. O., Cardoso, L. P., & Gonçalves, L. A. G. (2009). Influence of chemical interesterification on thermal behavior, microstructure, polymorphism and crystallization properties of canola oil and fully hydrogenated cottonseed oil blends. *Food Research International*, 42(8), 1153–1162.
- Ribeiro, A. P. B., Basso, R. C., Grimaldi, R., Gioielli, L. A., & Gonçalves, L. A. G. (2009). Instrumental methods for the evaluation of interesterified fats. *Food Analytical*

- Methods, 2(4), 282–302.
- Rietveld, H. (1967). Line profiles of neutron powder-diffraction peaks for structure refinement. *Acta Crystallographica*, 22(1), 151–152.
- Rozner, S., Popov, I., Uvarov, V., Aserin, A., & Garti, N. (2009). Templated cocrystallization of cholesterol and phytosterols from microemulsions. *Journal of Crystal Growth*, 311(16), 4022–4033.
- Ruland, W. (1961). X-ray determination of crystallinity and diffuse disorder scattering. *Acta Crystallographica*, 14(11), 1180–1185.
- Sagiri, S., Singh, V. K., Pal, K., Banerjee, I., & Basak, P. (2015). Stearic acid based oleogels: A study on the molecular, thermal and mechanical properties. *Materials Science and Engineering: C*, 48, 688–699.
- Shahzad, N., Khan, W., Shadab, M., Ali, A., Saluja, S. S., Sharma, S., & Abdel-Wahab, A. F. (2017). Phytosterols as a natural anticancer agent: Current status and future perspective. *Biomedicine & Pharmacotherapy*, 88, 786–794.
- Sintang, B., Dona, M., Rimaux, T., Van de Walle, D., Dewettinck, K., & Patel, A. R. (2017). Oil structuring properties of monoglycerides and phytosterols mixtures. *European Journal of Lipid Science and Technology*, 119(3).
- Sintang, M. D. B., Danthine, S., Brown, A., Van de Walle, D., Patel, A. R., Tavernier, I., & Dewettinck, K. (2017). Phytosterols-induced viscoelasticity of oleogels prepared by using monoglycerides. *Food Research International*, 100, 832–840.
- Sonoda, T., Takata, Y., Ueno, S., & Sato, K. (2004). DSC and synchrotron-radiation X-ray diffraction studies on crystallization and polymorphic behavior of palm stearin in bulk and oil-in-water emulsion states. *Journal of the American Oil Chemists' Society*, 81(4), 365–373.
- Tan, C., & Man, Y. (2002). Comparative differential scanning calorimetric analysis of vegetable oils: I. Effects of heating rate variation. *Phytochemical Analysis*, 13(3), 129–141.
- Toby, B. H. (2006). R factors in Rietveld analysis: How good is good enough? *Powder Diffraction*, 21(1), 67–70.
- USDA, U. (2010). *Dietary guidelines for Americans*. Washington, DC: US Department of Agriculture, US Department of Health and Human Services.
- Vaikousi, H., Lazaridou, A., Biliaderis, C. G., & Zawistowski, J. (2007). Phase transitions, solubility, and crystallization kinetics of phytosterols and phytosterol– Oil blends. *Journal of Agricultural and Food Chemistry*, 55(5), 1790–1798.
- Vonk, C. G. (1973). Computerization of Ruland's X-ray method for determination of crystallinity in polymers. *Journal of Applied Crystallography*, 6(Apr1), 148–152.
- Wu, T., Fu, J., Yang, Y. X., Zhang, L. S., & Han, J. H. (2009). The effects of phytosterols/stanols on blood lipid profiles: A systematic review with meta-analysis. *Asia Pacific Journal of Clinical Nutrition*, 18(2), 179–186.
- Yang, D. X., Chen, X. W., & Yang, X. Q. (2017). Phytosterols-based Oleogels self-assembled with Monoglyceride for controlled volatile release. *Journal of the Science of Food and Agriculture*, 98(2), 582–589.
- Yang, S., Li, G., Saleh, A. S., Yang, H., Wang, N., Wang, P., & Xiao, Z. (2017). Functional characteristics of Oleogel prepared from sunflower oil with  $\beta$ -Sitosterol and stearic acid. *Journal of the American Oil Chemists' Society*, 94(9), 1153–1164.
- Young, R. A. (1993). *The Rietveld method*. Vol. 5. International Union of Crystallography.
- Zychowski, L. M., Logan, A., Augustin, M. A., Kelly, A. L., Zabara, A., O'Mahony, J. A., & Auty, M. A. (2016). Effect of phytosterols on the crystallization behavior of oil-in-water milk fat emulsions. *Journal of Agricultural and Food Chemistry*, 64(34), 6546–6554.